Geophysical Research Letters

RESEARCH LETTER
10.1029/2019GL086585

Frequency-Dependent Behavior of Zonal Jet Variability

Erik A. Lindgren[1], Aditi Sheshadri[1], and R. Alan Plumb[2]

[1]Department of Earth System Science, Stanford University, Stanford, CA, USA, [2]Department of Earth, Atmospheric and Planetary Sciences, Massachusetts Institute of Technology, Cambridge, MA, USA

Key Points:
- Southern Hemisphere annular modes show similar spatial features under time filtering
- Cancellation of storm track signatures in first annular mode at low/high frequencies explains weak signal in total
- At periods greater than 30 days, the first annular mode explains shifts of both the jet and storm tracks

Correspondence to:
E. A. Lindgren,
ealindgr@stanford.edu

Citation:
Lindgren, E. A., Sheshadri, A., & Plumb, R. A. (2020). Frequency-dependent behavior of zonal jet variability. *Geophysical Research Letters*, *47*, e2019GL086585. https://doi.org/10.1029/2019GL086585

Received 6 DEC 2019
Accepted 3 MAR 2020
Accepted article online 12 MAR 2020

Abstract Recent work suggests that storm track diagnostics such as eddy heat fluxes and eddy kinetic energies have very small signatures in the first annular mode of zonal mean zonal wind, suggesting a lack of co-variability between the locations of the extratropical jet and storm tracks. The frequency-dependence of this apparent decoupling is explored in ERA-Interim reanalysis data. The annular modes show similar spatial characteristics in the different frequency ranges considered. Cancellation between the signatures of storm track diagnostics in the leading low-pass and high-pass filtered annular modes is evident, partly explaining their small signature in the total. It is shown that at timescales greater than 30 days, the first zonal wind mode describes latitudinal shifts of both the midlatitude jet and its associated storm tracks, and it appears that the persistence of zonal wind anomalies is sustained primarily by a baroclinic feedback.

1. Introduction

The leading modes of variability of the extratropical circulation are referred to as "annular modes" (see, e.g., Thompson & Wallace, 2000; Thompson, Wallace, & Hegerl, 2000) and are often derived using Empirical Orthogonal Function (EOF) analysis of meteorological fields such as geopotential height and zonal mean zonal wind. Limpasuvan and Hartmann (1999, 2000) and Lorenz and Hartmann (2001, 2003) described the eddy-mean flow interactions that maintain the annular modes. Karoly (1990), Hartmann and Lo (1998), and Lorenz and Hartmann (2001), among others, have argued that in the Southern Hemisphere, there is a positive feedback between high frequency (synoptic) eddies and the zonal mean flow. In each hemisphere, the leading EOF of zonal wind takes the form of a dipolar structure centered on the mean jet which, alone, would describe latitudinal fluctuations of the jet. The second EOF peaks at the maximum of the mean jet, with reversed sign in its wings; alone, this component describes intensification and narrowing of the jet. However, these patterns are not mutually independent, and together, they describe the poleward propagation of jet anomalies (James & Dodd, 1996; Feldstein, 1998; Lee et al., 2007; Sheshadri & Plumb, 2017) through nonzero lag-correlations (e.g., Sparrow et al., 2009).

Thompson and Woodworth (2014) and Thompson and Barnes (2014) argued that variability in the Southern Hemisphere extratropical zonal flow could be described in terms of two distinct structures: a barotropic annular mode (the Southern Annular Mode [SAM], derived from EOF analysis of zonal mean zonal wind), and a baroclinic annular mode (the BAM, the leading EOF of eddy kinetic energy [EKE]). The former dominates the variability in zonal mean kinetic energy and momentum fluxes, while the latter dominates the variability in EKE and eddy fluxes of heat; conversely, the eddy heat fluxes and EKEs associated with the SAM explain very small fractions of the total variance in their respective fields, while the BAM accounts for only a small fraction of the variance in the wave fluxes of momentum. These studies suggest that this decoupling between the wave fluxes of heat and momentum associated with the SAM and the BAM imply independent barotropic and baroclinic variations of the storm tracks, respectively. They also appear to have implications for the nature of eddy-mean flow interactions in SAM dynamics, since in some theories the baroclinic feedback is seen as critical to the mechanism of jet fluctuations (Hartmann, 2007; Robinson, 1994, 1996).

Sparrow et al. (2009) used a dynamical core model to examine the behavior of the two leading zonal wind EOFs. Given the separation of characteristic timescales between the eddy forcing and the zonal wind (Lorenz & Hartmann, 2001), they used a 30-day cutoff to distinguish high and low frequencies and showed that their model's annular modes behave differently at low and high frequencies. Blanco-Fuentes and Zurita-Gotor (2011) used reanalysis data to investigate the internal variability of baroclinicity in the Southern Hemisphere

midlatitudes and suggested that at high frequencies, variations in eddy heating dominate, while at low frequencies, this variability is forced by eddy momentum flux and surface friction. Distinct behavior of the Northern Hemisphere storm tracks at high and low frequencies has also been noted in several recent studies (e.g., Novak et al., 2015, 2017).

Recently, Boljka et al. (2018) investigated the relationships between the first EOFs of zonal mean zonal wind and EKE under time filtering in a dry dynamical core model as well as in reanalysis data. Although Thompson and Woodworth (2014) found that the SAM and EOF1 of EKE were largely decoupled, Boljka et al. (2018) showed that the SAM and EOF2 of EKE, which has a dipolar structure similar to the SAM, were strongly correlated (anticorrelated) in both their model and reanalysis data when the fields were low-pass (high-pass) filtered. The results of Boljka et al. (2018) therefore indicated that EKE shifts along with the SAM on long timescales.

In this paper, we use ERA-Interim reanalysis data (Dee et al., 2011) to explore the extent to which diagnostics of the storm tracks (heat fluxes and EKE) co-vary with the SAM at timescales of relevance to the climate change problem. We follow Sparrow et al. (2009) in using a 30-day cutoff to distinguish high and low frequencies. This temporal filtering is intended to separate different dynamical regimes. For periods less than about 30 days, one is resolving the baroclinic life cycles and thus highlighting an essentially transient mutual interaction between the eddies and the mean flow. At longer periods, the eddies may respond to jet changes in a quasi-steady manner while the mean flow may respond to the eddy variability as to a forcing that is stochastic in time. We do indeed find different characteristics in the two frequency bands: that cancellation between low- and high-frequency signals contribute to the weak correlation between the SAM, EKE, and heat flux and that the low-frequency SAM signals are much more in keeping with ideas of baroclinic feedback than appears to be the case in the absence of filtering. Thus, we show that on timescales of relevance to climate change, diagnostics of the storm tracks such as heat fluxes and EKE do co-vary with the zonal mean winds.

2. Method

We use daily mean ERA-Interim reanalysis data (Dee et al., 2011) from 1979 through 2018, with a horizontal resolution of 1.0° in latitude and longitude and 21 vertical levels between 100 and 1,000 hPa. Zonal mean zonal wind $(\overline{u})$, EKE $\left(\frac{1}{2}\left[u'^2+v'^2\right]\right)$, heat flux $\left(\overline{v'T'}\right)$, momentum flux $\left(\overline{u'v'}\right)$, and quasi-geostrophic Eliassen-Palm (EP) flux divergence are calculated. Bars denote zonal means, and primes represent deviations from the zonal mean. EKE, heat flux, and momentum flux are calculated from four-times daily resolution and then averaged over 24 hr. EOFs of zonal mean zonal wind are calculated from pressure and latitude weighted data between 90°S and 20°S and 100 and 1,000 hPa.

Following Sparrow et al. (2009), we separate the timescales that are comparable with those of baroclinic eddy life cycles from the longer timescales. To this end, we apply a Lanczos filter to the zonal wind. EOFs are calculated separately from the unfiltered, low-pass filtered, and high-pass filtered data. For all results shown here, we follow Sparrow et al. (2009) in using a 30-day cutoff for the filtering. The major characteristics of the results are insensitive to choices between 20 and 60 days; using a 10-day cutoff has a more profound impact.

3. Regressions on the Annular Modes

The Southern Hemisphere annual mean zonal mean zonal wind and EKE are shown in Figure 1. The subtropical and eddy-driven tropospheric jets (Figure 1a) are almost separated, with the latter peaking around 48°S; EKE (Figure 1b) has a broad upper tropospheric maximum encompassing both jets, but peaking around the latitude of the eddy-driven jet.

The two leading EOFs of zonal mean zonal wind are shown in Figure 2 for the unfiltered data as well as for the low-pass and high-pass filtered data. In the unfiltered data (left column), these two EOFs exhibit the characteristics noted by Lorenz and Hartmann (2001) and Sparrow et al. (2009), among others, with EOF1 being dominated by a dipole straddling the climatological midlatitude jet, with a weak tertiary maximum on the equatorward edge of the subtropical jet, while EOF2 is in quadrature with EOF1, with its primary extremum coincident with the climatological jet. Together, as discussed in Lorenz and Hartmann (2001) and Sheshadri and Plumb (2017), these modes describe the poleward propagation of zonal wind anomalies noted

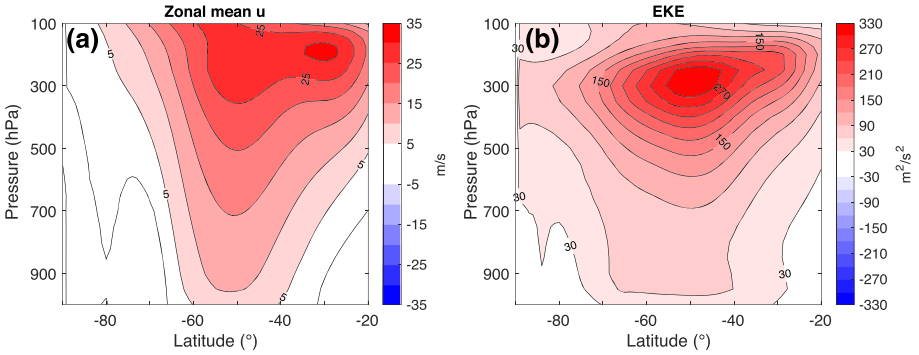

Figure 1. Annual mean (a) zonal mean zonal wind and (b) EKE in Southern Hemisphere. EKE = eddy kinetic energy.

in the atmosphere by Feldstein (1998) and in models by James and James (1992). The EOF structures are remarkably robust to the time filtering (as noted by Hartmann & Lo, 1998): the low- and high-pass-filtered EOFs are very similar to those of the unfiltered case, and EOF1 has a node near the climatological midlatitude jet maximum around 50°S in all cases, with extrema in the middle and upper troposphere at around 60°S and 40°S, with a weaker tertiary peak near 25°S, while EOF2 peaks near the midlatitude jet maximum around 50°S. Only EOF2 of the low-pass filtered data (Figure 2e) exhibits any significant departure from the unfiltered case, with a slightly more equatorward primary extremum, a weaker poleward extremum, and an equatorward extremum that is both stronger and further equatorward than its unfiltered counterpart.

Regressions against EOF1 (i.e., the SAM) of zonal mean zonal wind, EKE, and eddy heat and momentum fluxes are shown for unfiltered, low-pass, and high-pass data (including the sum of the latter two) in Figure 3. Since the regressions are made against the principal component of $\overline{u}$ in the relevant frequency band, the low- and high-pass regressions are not strictly additive although, given the similarity of the first two EOFs, they are approximately so. Panels (a) through (d) show that regressions of $\overline{u}$ onto EOF1 are very similar in structure for all four cases, indicating that the low- and high-pass filtered data as well as their sum describe SAM-like jet shifts. In the unfiltered data, EKE shows two upper level maxima and minima,

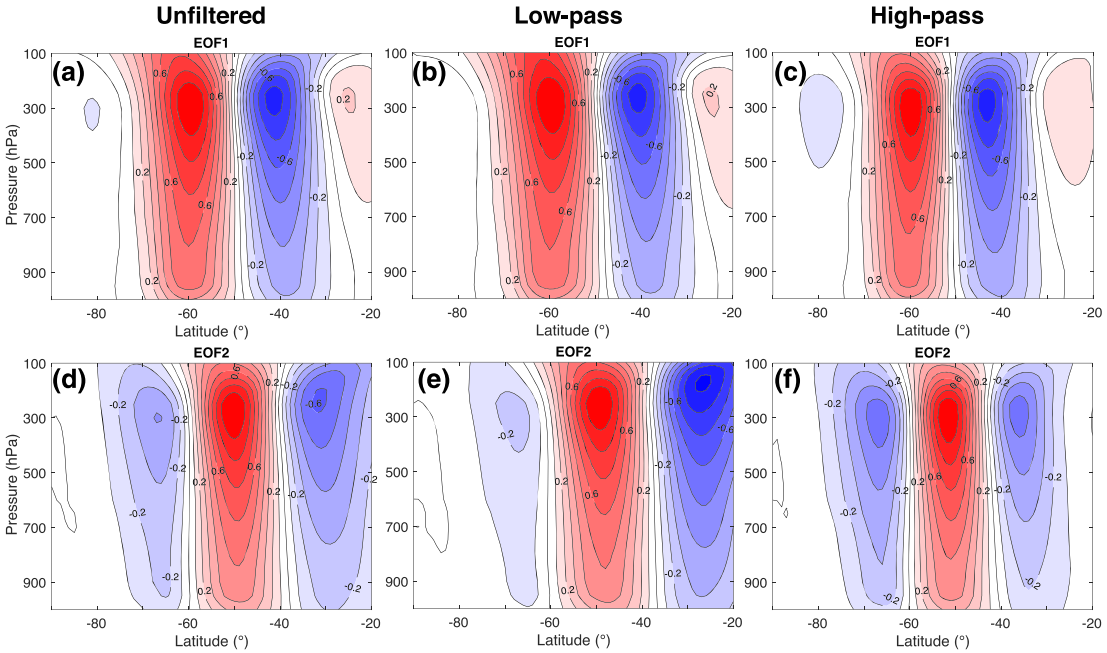

Figure 2. Latitude-pressure structure of the leading two EOFs of zonal mean zonal wind. EOF1 is shown in the top row; EOF1 based on unfiltered data in the left column (explains 45% of variance), 30-day low-pass filtered data in the middle column (explains 53% of low-pass filtered variance), and 30-day high-pass filtered data in the right column (explains 34% of high-pass filtered variance). The structure of EOF2 for the unfiltered (24%), 30-day low-pass (23%), and 30-day high-pass (28%) filtered data is shown in the bottom row. EOF = Empirical Orthogonal Function.

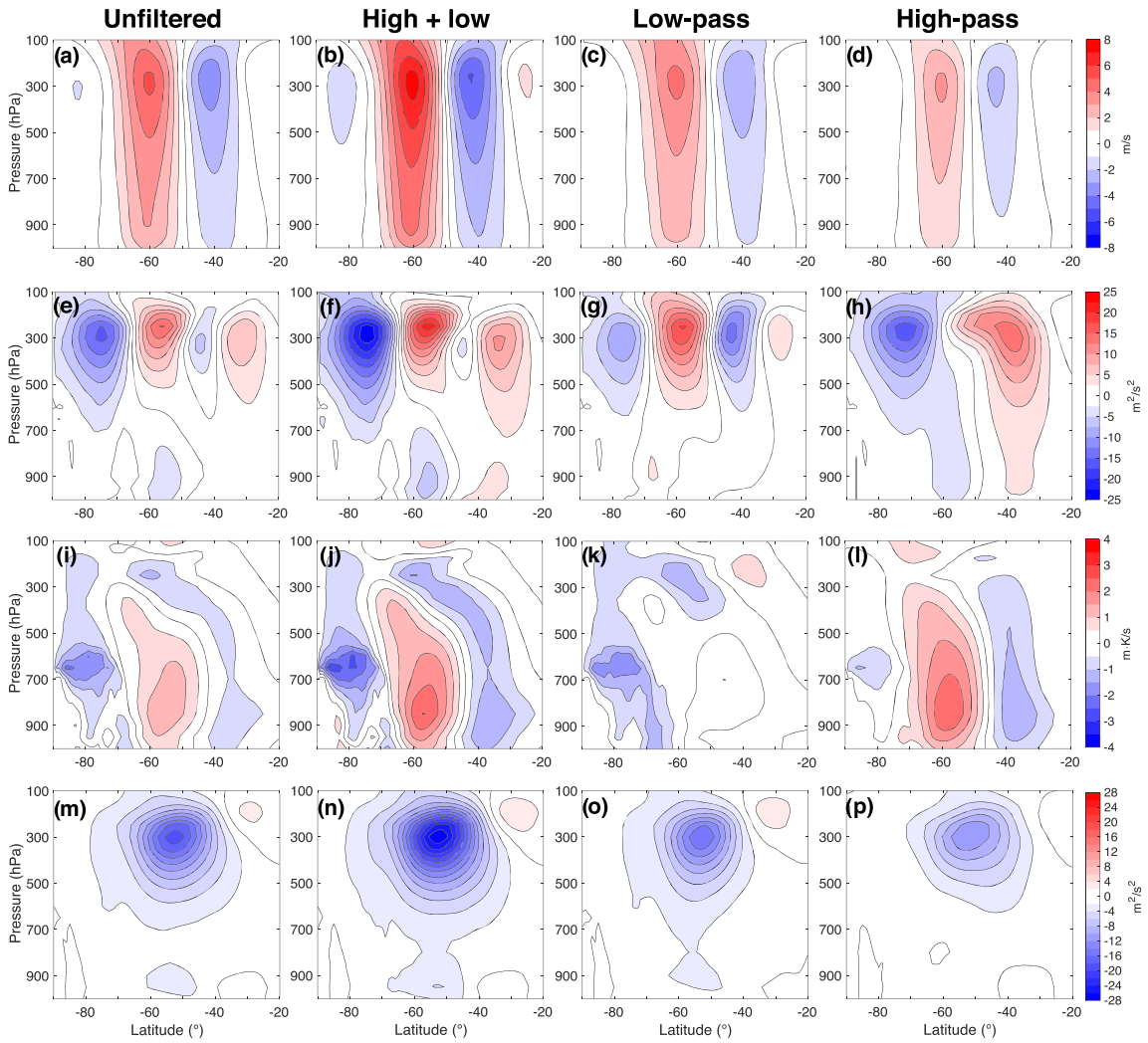

Figure 3. Regressions onto EOF1 of zonal mean zonal wind (top row), EKE (second row), eddy heat flux (third row) and eddy momentum flux (bottom row). Left column shows regressions onto unfiltered data, third column shows regressions onto 30-day low-pass filtered data, fourth column shows regressions onto 30-day high-pass filtered data, and the second column shows the sums of low- and high-pass filtered data. Contour intervals are 1 m/s (top row), 2.5 m^2/s^2, 0.5 $m \cdot K/s$ (third row), and 2 m^2/s^2, (bottom row). EKE = eddy kinetic energy, EOF = Empirical Orthogonal Function.

with the strongest minimum located closer to the pole (Figure 3e). Thompson and Woodworth (2014), who analyzed ERA-Interim data from 1979 through 2010, obtained practically identical patterns when regressing EKE onto the SAM (see Figure 2e in their paper). While a local maximum and a (weak) local minimum peak at latitudes close to the maximum and minimum in the regression of $\overline{u}$ onto EOF1 (Figure 3a), they are far from coincident. This suggests that, in the unfiltered case, the latitudinal structure of EKE does not co-vary with that of $\overline{u}$.

However, the low- and high-pass filtered data tell a very different story: in the low-pass filtered case (Figure 3g), the EKE regression shows a strong midlatitude dipole with increased (decreased) EKE coincident with westerly (easterly) wind anomaly, while the high-pass filtered case (Figure 3h) exhibits negative (positive) EKE anomalies poleward (equatorward) of about 55°S. The sum of the low- and high-pass filtered data (Figure 3f) has a structure very similar to that of the unfiltered case, although with extrema of higher magnitudes. All of the above shows (1) that the first zonal wind mode describes latitudinal shifts of both the midlatitude jet and its associated storm tracks at long timescales; (2) that EKE decreases in the direction of the jet shift and increases in the opposite direction at short timescales; and (3) that these two behaviors add up to the correlation seen in the unfiltered data, indicating that cancellation between low- and high-frequency processes produces the weak structural correspondence seen in Figure 3e. The first

two of these points are consistent with the strong correlation (anticorrelation) between the SAM and EOF2 of EKE under low-pass (high-pass) filtering shown by Boljka et al. (2018).

The eddy heat flux signal of unfiltered EOF1 (Figure 3i) has negative components in the lower troposphere over Antarctica and equatorward of about 45°S, and a positive component largely coincident with the positive lobe of the $\overline{u}$ signal. The low-pass filtered signal (Figure 3k) displays a slightly more negative surface heat flux between about 70°S and 60°S, close to the anomalous westerlies, and practically no positive components further equatorward, suggesting that increased low-level baroclinicity due to increased westerlies increase the eddy heat flux at longer timescales. The high-pass signal (Figure 3l), by contrast, is positively correlated in latitude with the zonal wind anomalies with more positive (negative) heat flux where the zonal wind anomalies are westerly (easterly), and thus spatially out of phase with the low-level baroclinicity. Therefore, at short timescales, the vertical wave flux moves equatorward when the zonal wind shifts poleward. As in the case of $\overline{u}$ and EKE, the sum of the low- and high-pass filtered signals (Figure 3j) results in a structure very similar to the unfiltered data but with extrema of larger magnitudes. EOF1 of heat flux is a monopole while EOF2 is a dipole (not shown), and for unfiltered, low-pass filtered as well as high-pass filtered heat flux data, the first two EOFs explain more than 50% of the total variance. In the unfiltered data, the first two EOFs of heat flux are largely decoupled from the SAM, with correlation magnitudes of 0.02 and 0.03 for EOF1 and EOF2, respectively. However, these correlations increase under filtering, with magnitudes of 0.31 and 0.04 for low-pass filtered data and 0.10 and 0.29 for high-pass filtered data.

The momentum flux pattern associated with unfiltered EOF1 is dominated by northward fluxes extending from about 40°S to 70°S; as has been noted frequently before (e.g., Hartmann & Lo, 1998; Karoly, 1990; Robinson, 1994), these fluxes act to reinforce the zonal wind anomalies. Unlike the heat fluxes, the low- and high-pass momentum fluxes are similar to each other, and to the total, the only difference being a slight equatorward displacement of the high-pass fluxes relative to the others.

4. Wave-Activity Budget

To understand what sets the frequency variability of EOF1, we consider the wave activity budget in the form of the generalized EP relation (e.g., Edmon et al., 1980), regressed onto EOF1 of low- and high-pass-filtered data:

$$\left\langle \frac{\partial A}{\partial t} \right\rangle + \langle \nabla \cdot \vec{F} \rangle = \langle D \rangle, \tag{1}$$

where $\langle\rangle$ denotes regression onto EOF1 of low- and high-pass filtered data, A is wave activity density, D represents non-conservative terms (friction, thermal damping, and wave breaking), and $\nabla \cdot \vec{F}$ is the divergence of EP flux. The latter is in spherical coordinates defined as

$$\nabla \cdot \vec{F} = -\frac{1}{\cos\phi}\frac{\partial}{\partial \phi}\left(\cos^2\phi \overline{u'v'}\right) + f r_0 \cos\phi \frac{\partial}{\partial p}\left(\frac{\overline{v'\theta'}}{\overline{\theta}_p}\right), \tag{2}$$

where r_0 is the radius of Earth, ϕ is latitude, f is the Coriolis parameter, and θ is potential temperature. Evaluated at a pressure level p_0 and slightly rearranged, equation (1) becomes

$$\int_0^{p_0} \left\langle \frac{\partial A}{\partial t} - D \right\rangle dp = \frac{1}{\cos\phi}\frac{\partial}{\partial \phi}\left(\cos^2\phi \int_0^{p_0} \langle \overline{u'v'} \rangle dp\right) - f r_0 \cos\phi \left\langle \frac{\overline{v'\theta'}}{\overline{\theta}_p} \right\rangle_{p=p_0}. \tag{3}$$

Figure 4 shows the two terms on the right hand side of equation (3) (i.e., $-\nabla \cdot \vec{F}$ vertically integrated to pressure level p_0) regressed onto EOF1 of unfiltered, low-pass and high-pass data (and the sum of the latter two) at three tropospheric pressure levels. The first term is the momentum flux component, and the second term is the heat flux component. If these terms are of equal magnitudes but opposite signs, there is no EP flux divergence above the given pressure level. The heat flux component is associated with baroclinic instability; in contrast, the momentum flux component would be dominant if the instability is barotropic.

The two terms have similar latitudinal structures in the unfiltered data (Figure 4a) and add up to EP flux convergence equatorward of about 45°S to 50°S and divergence poleward; the convergence and divergence

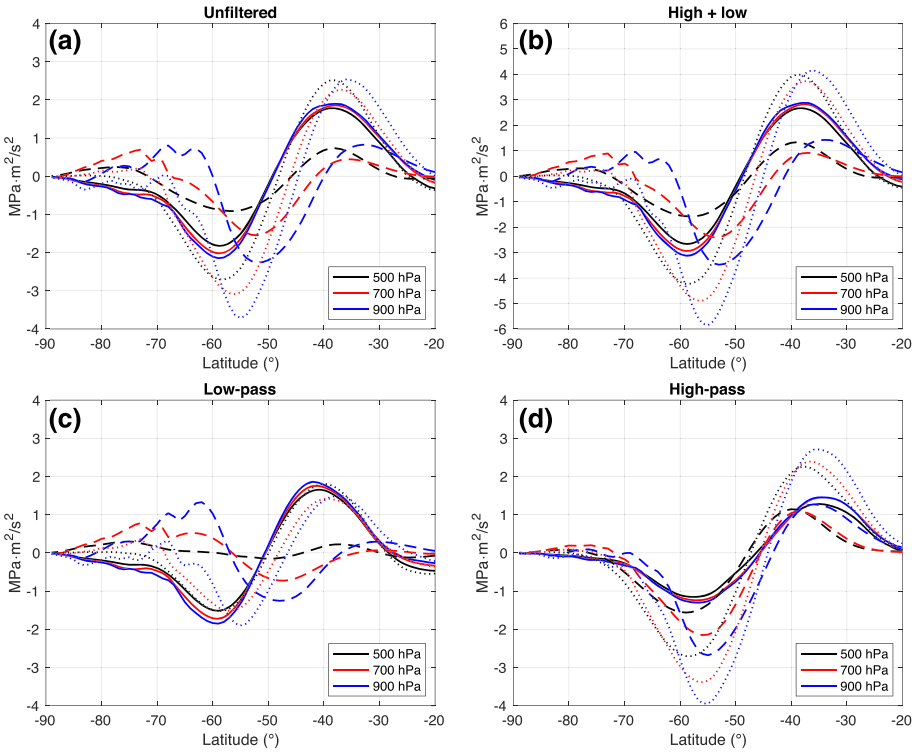

Figure 4. Momentum flux (solid) and heat flux (dashed) components of the right hand side of Equation (3) and their sum (dotted line) at three pressure levels. (a) Unfiltered data, (b) sum of low- and high-pass filtered data, (c) low-pass filtered data, and (d) high-pass filtered data.

is balanced by changes in the wave activity density and nonconservative processes. Keeping the sign difference in mind, the latitudinal structure of Figure 4a is in agreement with the heat flux anomalies found by Thompson and Woodworth (2014) during the decay stage of the SAM (see Figure 8c in their paper). As before, the sum of low- and high-pass filtered data (Figure 4b) matches the structure of the unfiltered data but with higher magnitudes.

However, nonconservative and transient effects play a much smaller role in the low-pass filtered data (Figure 4c). The signs of the momentum flux and heat flux components are largely anticorrelated in latitude, and the terms partly cancel each other out, resulting in EP flux convergences and divergences of magnitudes that are lower than the individual components at some latitudes. This balance suggests that the baroclinic (heat) fluxes play an important role in the low-frequency variability by feeding barotropic (momentum) fluxes. This is consistent with the idealized modeling results of Sparrow et al. (2009), who found that the horizontal and vertical eddy terms of EP flux reach a quasi-equilibrium at low frequencies, dominated by positive eddy feedback. The overall picture of the eddy signal associated with EOF1 at low frequency, therefore, is like that described by Robinson (1994) and Robinson (2000), and found by Boljka et al. (2018) in model and reanalysis data: a quasi-steady response of increased baroclinic wave generation, and locally increased EKE, in association with a poleward shift of the jet. In other words, baroclinic fluxes act to support the barotropic structure of the SAM at low frequencies.

In contrast, the signs of the momentum flux and heat flux components for high-pass-filtered data (Figure 4d) are strongly correlated in latitude, showing that the high-frequency variability is set by upper tropospheric wave breaking and changes in the wave activity density. This high frequency behavior is consistent with the results of Sparrow et al. (2009). While the momentum flux component is similar to that of the low-pass filtered case, the heat flux (baroclinic) component is very different, indicating that tropospheric heat flux leads to wave breaking and changes in wave activity density at short timescales.

5. Conclusions

The SAM displays a strong zonal wind component, corresponding to a shift of the midlatitude jet, and a clear signal in momentum flux. Its EKE signal represents a very small fraction of total EKE variability and is spatially rather weakly correlated with the zonal wind shift. However, characteristics of the modes appear somewhat different when separated into components with periods less than, and greater than, 30 days.

The EOFs show similar spatial zonal wind structures in the low-pass and high-pass ranges; nevertheless, the eddy signatures are in some cases very different. In the raw data, there is evidently some cancellation occurring between low-pass and high-pass contributions to EKE and eddy heat fluxes. At low frequencies, the eddy heat and momentum fluxes behave qualitatively as one might expect for zonal wind perturbations in steady state. In particular, EOF1 is associated with increased EKE coincident with the latitudes of anomalous westerlies and strengthened low-level baroclinicity. The relationship between the eddies and the jet is consistent with a quasi-steady perspective: enhanced eddy heat fluxes and EKE being largely coincident with a locally strengthened jet and enhanced low-level baroclinicity. Thus, maintenance of persistent zonal wind anomalies appears to result primarily from a baroclinic, rather than barotropic, feedback mechanism. Correlation coefficients between the SAM and first two components of heat flux show that while the magnitude of the correlation in unfiltered data is low, it increases dramatically with filtering.

At high frequencies, upper tropospheric wave breaking and transient effects, as opposed to heat and momentum flux contributions, dominate the wave activity budget, and high-frequency signatures of EKE and heat flux exhibit maxima (minima) at latitudes where their low-frequency counterparts show minima (maxima). The high- and low-frequency signals of zonal mean zonal wind, EKE, heat flux, and momentum flux add up to structures remarkably similar to the signals found in unfiltered data, indicating that cancellations between high- and low-frequency processes result in the weak SAM signals observed in raw data.

Thompson and Woodworth (2014) and Thompson and Barnes (2014) have argued that Southern Hemisphere extratropical flow can be described by the SAM (a barotropic mode) and the first EOF of EKE (a baroclinic mode) and that the SAM accounts for a very small fraction of EKE and heat flux variability. However, Boljka et al. (2018) showed that strong correlations between the SAM and EOF2 of EKE can be found under time filtering. Here we confirm the results of Boljka et al. (2018) by showing that the correlations between the SAM, EKE, and heat flux depend strongly on the timescale one considers. Additionally, we demonstrate that the weak correlations between these variables in unfiltered data are partly due to cancellation between low- and high-frequency signals. At longer timescales of relevance to the climate change problem, SAM variability seems to be largely maintained by baroclinic, rather than barotropic, mechanisms.

Acknowledgments
This work was partially supported by the National Science Foundation through grant AGS-1921409 to Stanford University, and a Junior Fellow Award from the Simons Foundation to AS. Part of the work was done during an extended visit by RAP to the University of Reading, with support provided by the Department of Meteorology Visitors Programme. We acknowledge helpful discussions and communications with Michael Blackburn, Ted Shepherd, Sarah Sparrow, Dave Thompson, and Paul Kushner. ERA-Interim reanalysis data are available through ECMWF.

References

Blanco-Fuentes, J., & Zurita-Gotor, P. (2011). The driving of baroclinic anomalies at different timescales. *Geophysical Research Letters*, *38*(23), L23805. https://doi.org/10.1029/2011GL049785

Boljka, L., Shepherd, T. G., & Blackburn, M. (2018). On the coupling between barotropic and baroclinic modes of extratropical atmospheric variability. *Journal of the Atmospheric Sciences*, *75*(6), 1853–1871. https://doi.org/10.1175/JAS-D-17-0370.1

Dee, D. P., Uppala, S. M., Simmons, A. J., Berrisford, P., Poli, P., Kobayashi, S., et al. (2011). The Era–Interim reanalysis: Configuration and performance of the data assimilation system. *Quarterly Journal of the Royal Meteorological Society*, *137*(656), 553–597. https://doi.org/10.1002/qj.828

Edmon, H. J., Hoskins, B. J., & McIntyre, M. E. (1980). Eliassen–palm cross sections for the troposphere. *Journal of the Atmospheric Sciences*, *37*(12), 2600–2616. https://doi.org/10.1175/1520-0469(1980)037<2600:EPCSFT>2.0.CO;2

Feldstein, S. B. (1998). An observational study of the intraseasonal poleward propagation of zonal mean flow anomalies. *Journal of the Atmospheric Sciences*, *55*(15), 2516–2529. https://doi.org/10.1175/1520-0469(1998)055<2516:AOSOTI>2.0.CO;2

Hartmann, D. L. (2007). The atmospheric general circulation and its variability. *Journal of the Meteorological Society of Japan*, *85B*, 123–143. https://doi.org/10.2151/jmsj.85B.123

Hartmann, D. L., & Lo, F. (1998). Wave–driven zonal flow vacillation in the southern hemisphere. *Journal of the Atmospheric Sciences*, *55*(8), 1303–1315. https://doi.org/10.1175/1520-0469(1998)055<1303:WDZFVI>2.0.CO;2

James, I. N., & Dodd, J. P. (1996). A mechanism for the low–frequency variability of the mid–latitude troposphere. *Quarterly Journal of the Royal Meteorological Society*, *122*(533), 1197–1210. https://doi.org/10.1002/qj.49712253309

James, I. N., & James, P. M. (1992). Spatial structure of ultra–low–frequency variability of the flow in a simple atmospheric circulation model. *Quarterly Journal of the Royal Meteorological Society*, *118*(508), 1211–1233. https://doi.org/10.1002/qj.49711850810

Karoly, D. J. (1990). The role of transient eddies in low–frequency zonal variations of the southern hemisphere circulation. *Tellus A: Dynamic Meteorology and Oceanography*, *42*(42A), 41–50. https://doi.org/10.3402/tellusa.v42i1.11858

Lee, S., Son, S.-W., Grise, K., & Feldstein, S. B. (2007). A mechanism for the poleward propagation of zonal mean flow anomalies. *Journal of the Atmospheric Sciences*, *64*(3), 849–868. https://doi.org/10.1175/JAS3861.1

Limpasuvan, V., & Hartmann, D. L. (1999). Eddies and the annular modes of climate variability. *Geophysical Research Letters*, *26*(20), 3133–3136. https://doi.org/10.1029/1999GL010478

Limpasuvan, V., & Hartmann, D. L. (2000). Wave–maintained annular modes of climate variability. *Journal of Climate*, *13*(24), 4414–4429. https://doi.org/10.1175/1520-0442(2000)013<4414:WMAMOC>2.0.CO;2

Lorenz, D. J., & Hartmann, D. L. (2001). Eddy–zonal flow feedback in the southern hemisphere. *Journal of the Atmospheric Sciences*, *58*(21), 3312–3327. https://doi.org/10.1175/1520-0469(2001)058<3312:EZFFIT>2.0.CO;2

Lorenz, D. J., & Hartmann, D. L. (2003). Eddy–zonal flow feedback in the northern hemisphere winter. *Journal of Climate*, *16*(8), 1212–1227. https://doi.org/10.1175/1520-0442(2003)16<1212:EFFITN>2.0.CO;2

Novak, L., Ambaum, M. H. P., & Tailleux, R. (2015). The life cycle of the north atlantic storm track. *Journal of the Atmospheric Sciences*, *72*(2), 821–833. https://doi.org/10.1175/JAS-D-14-0082.1

Novak, L., Ambaum, M. H. P., & Tailleux, R. (2017). Marginal stability and predator prey behaviour within storm tracks. *Quarterly Journal of the Royal Meteorological Society*, *143*(704), 1421–1433. https://doi.org/10.1002/qj.3014

Robinson, W. A. (1994). Eddy feedbacks on the zonal index and eddy–zonal flow interactions induced by zonal flow transience. *Journal of the Atmospheric Sciences*, *51*(17), 2553–2562. https://doi.org/10.1175/1520-0469(1994)051<2553:EFOTZI>2.0.CO;2

Robinson, W. A. (1996). Does eddy feedback sustain variability in the zonal index? *Journal of the Atmospheric Sciences*, *53*(23), 3556–3569. https://doi.org/10.1175/1520-0469(1996)053<3556:DEFSVI>2.0.CO;2

Robinson, W. A. (2000). A baroclinic mechanism for the eddy feedback on the zonal index. *Journal of the Atmospheric Sciences*, *57*(3), 415–422. https://doi.org/10.1175/1520-0469(2000)057<0415:ABMFTE>2.0.CO;2

Sheshadri, A., & Plumb, R. A. (2017). Propagating annular modes: Empirical orthogonal functions, principal oscillation patterns, and time scales. *Journal of the Atmospheric Sciences*, *74*(5), 1345–1361. https://doi.org/10.1175/JAS-D-16-0291.1

Sparrow, S., Blackburn, M., & Haigh, J. D. (2009). Annular variability and eddy–zonal flow interactions in a simplified atmospheric gcm. Part I: Characterization of high– and low–frequency behavior. *Journal of the Atmospheric Sciences*, *66*(10), 3075–3094. https://doi.org/10.1175/2009JAS2953.1

Thompson, D. W. J., & Barnes, E. A. (2014). Periodic variability in the large–scale southern hemisphere atmospheric circulation. *Science*, *343*(6171), 641–645. https://doi.org/10.1126/science.1247660

Thompson, D. W. J., & Wallace, J. M. (2000). Annular modes in the extratropical circulation. Part I: Month-to-month variability. *Journal of Climate*, *13*(5), 1000–1016. https://doi.org/10.1175/1520-0442(2000)013<1000:AMITEC>2.0.CO;2

Thompson, D. W. J., Wallace, J. M., & Hegerl, G. C. (2000). Annular modes in the extratropical circulation. Part II: Trends. *Journal of Climate*, *13*(5), 1018–1036. https://doi.org/10.1175/1520-0442(2000)013h1018:AMITECi2.0.CO;2

Thompson, D. W. J., & Woodworth, J. D. (2014). Barotropic and baroclinic annular variability in the southern hemisphere. *Journal of the Atmospheric Sciences*, *71*(4), 1480–1493. https://doi.org/10.1175/JAS-D-13-0185.1